Vol. 18, No. 3 (2019) 995-1015
Revista Mexicana de Ingeniería Química

CFD ASSISTED ANALYSIS AND DESIGN OF HYDRAULIC FLOCCULATORS
ANÁLISIS Y DISEÑO ASISTIDO POR CFD DE FLOCULADORES HIDRÁULICOS

C.E. Llano-Serna, J.A. Coral-Portillo, J. Fontalvo, O.A. Prado-Rubio*

Departamento de Ingeniería Química, Universidad Nacional de Colombia, Campus La Nubia, km 9 vía al Aeropuerto La Nubia, Bloque L, Manizales, Colombia.

Received: September 18, 2018; Accepted: November 20, 2018

Abstract

In water treatment processes, the hydrodynamic behavior in a flocculation unit is critical in order to achieve flocs with appropriate characteristics that allow their subsequent separation. In this contribution computational fluid dynamics (CFD) was used to investigate the flow characteristics of a Cox type hydraulic flocculator at the water purification plant in Viterbo, Colombia. In order to improve the original design, the effect of the windows configurations and the inlet volumetric flow was investigated. For the configurations performance assessment, the local velocity gradient and residence time distribution were calculated. The simulation results indicate that the window position have a considerable effect on the velocity gradient and retention time distribution, while the number of windows showed a negligible effect on the retention time. It was possible to decrease the local gradient mean error between 10 and 20% by employing 2 windows instead of 1. The best hydrodynamic performance was obtained by locating the windows horizontally aligned and using 2 windows between chambers. These results are encouraging to systematically improve the plant design thus performance.

Keywords: flocculation, computational fluid dynamics, drinking water treatment.

Resumen

En los procesos de tratamiento de agua, el comportamiento hidrodinámico en las unidades de floculación es crítico para conseguir partículas de características adecuadas, que permitan su posterior separación. En esta contribución se empleó dinámica de fluidos computacional (CFD) para investigar las características del flujo en un floculador hidráulico tipo Cox ubicado en la planta de potabilización de agua de Viterbo, Colombia. En aras de mejorar el diseño original, se investigó el efecto de la configuración de las ventanas y del flujo volumétrico de entrada. Para valorar el desempeño de las configuraciones, se estimaron los gradientes locales de velocidad y la distribución del tiempo de residencia. Los resultados de las simulaciones indicaron que la posición de los pasajes puede tener efectos considerables en la distribución del gradiente de velocidad y el tiempo de retención. Si bien el número de ventanas mostró un efecto insignificante sobre el tiempo de retención, fue posible disminuir el error medio del gradiente local entre 10 y 20%, al emplear 2 pasajes en lugar de 1. El mejor rendimiento hidrodinámico se obtuvo ubicando las ventanas alineadas horizontalmente y usando 2 ventanas entre cámaras. Estos resultados son alentadores para mejorar sistemáticamente el diseño de la planta y por lo tanto su rendimiento.

Palabras clave: floculación, dinámica de fluidos computacional, tratamiento de agua potable.

1 Introduction

In low and middle income countries a mean of 12% of the population uses drinking water directly from unimproved sources without any purification treatment. As a result of the poor water quality caused by factors as pollution, 502,000 deaths were attributed to unsafe and insufficient drinking water in 2012 (World Health Organization, 2014). In order to overcome this water public health issue, the water potabilization plants should be designed and operated in an economic and efficient way, guaranteeing at the same time a secure and continuous supply of water with an adequate quality for consumption and domestic use (Romero-Rojas, 2006). Among the units operation that are part of water potabilization process, coagulation and flocculation are extremely important. These are also essential in others areas as the biochemistry and waste water treatment (Bratby, 2016). The main purpose of these processes is to agglomerate the particles that are present in the water

* *Corresponding author. E-mail*: oaprador@unal.edu.co
https://doi.org/10.24275/uam/izt/dcbi/revmexingquim/2019v18n3/Llano
issn-e: 2395-8472

as colloids or solution. Thus, remove them using solid-liquid separation process as filtration or sedimentation. Through the processes, the flocs acquire the adequate size and characteristics to be retained in the filter and achieve an adequate settling velocity in the sedimetator (Cheremisinoff, 2002; Pérez-Parra, 2006).

The colloids surface possess an electric charged surface, which produce repulsive forces between these particles, keeping them as a suspension (Sharma, 2007; Bratby, 2016). In the coagulation stage the particles are destabilized by means of the addition of a substance (coagulant) that allows to reduce the colloids surface electric charge. Then, the agglutinated particles (so called flocs) are obtained by the aggregation of the destabilized particles. In the process, the coagulant addition should be accompanied of a rapid mixing stage, in order to achieve a rapid and uniform mixing. Subsequently, an additional process where the particles are induced to get closer to each other is required (Romero-Rojas, 2006). The probability of collision between coagulated particles can be increased improving the particles transport (Pérez-Parra, 2006; Bratby, 2016). In a flocculator, the particle transport is enhanced by means of velocity gradients which can be induced in the fluid by means of mechanical stirrers (mechanical flocculators) or by using the available hydraulic energy through the headloss in the structure (hydraulic flocculators). Hydraulic flocculators do not require electrical equipment. This gives rise to a lower power consumption, a minimum maintenance requirement and invulnerability to electrical failures. However, in comparison with the mechanical flocculators, these usually require a largest installation area and allow a reduced control flexibility of the degree of mixing (Pérez-Parra, 2006; Romero-Rojas, 2006). In some cases, different types of flocculants as responsive polymers (Contreras-Andrade *et al*., 2015) or environmentally friendly agents based on starches (López-Vidal *et al*., 2014), among others, are added in order to improve the flocculation performance.

The most common hydraulic flocculators are the horizontal and vertical baffled flocculators (Romero-Rojas, 2006). However, alternative designs have also been proposed, as the Cox flocculators. Those are widely used in Latin-America and in comparison with the baffled flocculators usually occupy a lower space. A Cox flocculator is composed of different chambers of square horizontal section connected in series. The water enters and leaves the chambers through windows located in the top and bottom of each chamber alternately. In this way, the flow ascend in a chamber and descend in the next one. In both hydraulic and mechanical flocculators, the velocity gradient is decreased gradually as the fluid go through the chambers. In the Cox flocculators, the gradients are obtained due to the velocity that the water obtains when it pass through the windows. In order to obtain the gradual velocity decreasing, the windows transversal area is increased gradually (Pérez-Parra, 2006; Lozano-Rivas & Lozano-Bravo, 2015). It was found, in previous studies (Castellanos, 1982), that using two windows between chambers instead of one, could increase notably the flocculation efficiency. Besides, the windows shape does not affect the process appreciably (Lozano-Rivas & Lozano-Bravo, 2015).

The flocculation performance can be affected by different factors as pH, temperature and input floc size and concentration. As the effect of these variables has not been fully theoretically defined, a previous experimental test is necessary in order to find the best operation condition, for a certain water quality. During operation, water characteristics could also change markedly depending of factors as the supply, pollution and climatological factors (Romero-Rojas, 2006). Therefore, the mean velocity gradient and the retention time are the process main variables, since these both are the most manipulable (Pérez-Parra, 2006). Specifically, retention times shorter than the optimal are not enough for a complete floc formation, while long periods could increase the floc rupture. On other hand, low velocity gradients do not allow the particles to approach each other, while a high gradient could increase the hydrodynamic shear forces, which trigger the flocs rupture (Pérez-Parra, 2006; Romero-Rojas, 2006). The turbulence variation is critical, since the floc disintegration could occur in the system zones where the turbulence is excessive (Haarhoff & van der Walt, 2001). Therefore, ensuring that the optimal operation conditions are really obtained in the flocculation unit is necessary to obtain an appropriate flocculation.

For the aforementioned reasons, a detailed hydrodynamic characterization of these and all the water treatment units is very important. Conventionally, the design of the water treatment units is performed using the mean values of the required flow parameters and lumped design equations. On the other hand, the experimental determination of the flow characteristics is usually limited by the precision and the availability of adequate measurement systems (Pan *et al*., 2016). Therefore, by means of these conventional methods, the determination of the flow

parameters variability through the whole structure is not straightforward. However, computational fluid dynamics (CFD) has shown the potential to provide reliable results for problems with different types of fluid flow (Raffo-Durán *et al*., 2014) and consequently can assist this kind of characterization. The CFD approach can be applied to perform dynamic simulations of the hydrodynamic behavior through 3D structures, providing the necessary understanding about the flow distribution, velocity gradients and retention times. This makes it a valuable tool to economically and efficiently evaluate these systems and propose design and operational improvements (Norton & Sun, 2006). Although the advantages, these tools have not been exploited yet as it should (Daigger, 2011).

CFD has been used in other studies to investigate the hydrodynamic flocculators performance. Haarhoff & van der Walt (2001) employed CFD to optimize three geometrical design ratios of an around-the-end barriers hydraulic flocculator (horizontal baffled flocculator). As performance indicators, the Morril index, dispersion coefficient and the local gradient variability (with relation to the mean gradient) were used. They found that the highest impact is produced by the slot width ratio (with respect to the channel width between baffles), while the depth ratio effect at constant flow velocity was insignificant. Bridgeman *et al*. (2010) simulated a Laboratory scale flocculation jar tester and two full scale flocculators: a mechanical flocculator and a vertical baffled hydraulic flocculator. A significant difference in the local gradient distribution was found in all of them. They also identified recirculation loops and dead spots at the cells between baffles in the hydraulic flocculator. Vadasarukkai *et al*. (2011) evaluated through a CFD approach a three-stage tapered hydraulic flocculator used in a water treatment plant. Their study indicated an inadequate mixing in the flocculation tanks. The G-values decreased drastically from the first to the second tank while a minimum difference between the last two tanks was observed. Due to the existence of stagnant zones inside the tanks, a mean retention time lower than the theoretical was found. Mohammadighavam *et al*. (2016) used CFD to optimize a hydraulic flocculator used for the peat extraction runoff water treatment. In order to select between the best types of barrier designs and geometry designs ratios, the local velocity gradient value and distribution through the structure were employed as optimization parameters. The optimum range value found in jar tests were taken as basis. The around-the-end barriers hydraulic flocculator showed the best G-value uniformity. They stated that in order to obtain the desired velocity gradient, the geometry ratios should be adjusted, based on the design discharge. Oliveira & Teixeira (2017) evaluated different configurations of a helically coiled tube hydraulic flocculator. However, in order to characterize appropriately this kind of units (where the streamlines has a quasi-periodic behavior), they proposed a hydraulic parameter indicator based on representatives streamlines. In comparison with the velocity gradient, the proposed indicator showed a better adjustment with relation to the turbidity removal efficiency found experimentally.

Due to the high impact of the flow behavior on the flocculation efficiency and encouraging previous research, in this contribution it is desired to compare and evaluate the hydrodynamic behavior of a Cox flocculator under different geometry and inflow conditions by means of CFD, using the software COMSOL Multiphysics®. The local velocity gradients and retention times are also evaluated and compared. It has been shown that by means of this systems modeling, it is possible to find configurations that allow systematically improving the flocculation process performance. Since the Cox flocculators are common between the Latin-American communities, applying this approach leads to the improvement of the water treatment plants designs and a higher economic efficiency.

2 Methodology

2.1 CFD Simulations

2.1.1 Model

The simulations were performed in COMSOL Multiphysics® software, using the mixture model in turbulent flow with the *k-ε* turbulence model, due to the turbulent characteristics of the flow (70000 <Re< 120000 in the passages between chambers). This turbulence model has been used and validated in previous hydrodynamic studies of flocculation systems (Bridgeman *et al*., 2010; Vadasarukkai *et al*., 2011; Mohammadighavam *et al*., 2016). In order to describe the fluid dynamics, this approach uses a set of the Navier-Stockes equations for the mixture (Eq 1). The conservation of momentum equation is shown in Eq 1 and the mass conservation equation is shown in Eq 4 (assuming incompressible flow) (COMSOL

Multiphysics ®, 2017).

$$\rho\frac{\partial \mathbf{u}}{\partial t}+\rho(\mathbf{u}\cdot\nabla)\mathbf{u}=-\nabla P-\nabla\cdot\tau_{Gm}+\rho\mathbf{g}+\mathbf{F} -\nabla\cdot\left[\rho c_d(1-c_d)\left(\mathbf{u_{slip}}-\frac{D_{md}}{1-c_d}\frac{\nabla\phi_d}{\phi_d}\right)\left(\mathbf{u_{slip}}-\frac{D_{md}}{1-c_d}\frac{\nabla\phi_d}{\phi_d}\right)^T\right] \quad (1)$$

$$\tau_{Gm}=(\mu+\mu_T)\left[\nabla\mathbf{u}+(\nabla\mathbf{u})^T-\frac{2}{3}(\nabla\cdot\mathbf{u})\mathbf{I}\right]-\frac{2}{3}\rho k\mathbf{I} \quad (2)$$

$$D_{md}=\frac{\mu_T}{\rho\sigma_T} \quad (3)$$

$$(\rho_c-\rho_d)\left\{\nabla\cdot\left[\phi_d(1-c_d)\mathbf{u_{slip}}-D_{md}\nabla\phi_d\right]+\frac{m_{dc}}{\rho_d}\right\}+\rho_c(\nabla\cdot\mathbf{u})=0 \quad (4)$$

where t is the time, $\mathbf{u}$ is the mixture velocity vector, $\mathbf{u_{slip}}$ is the relative velocity vector between the two phases, ρ is the mixture density, μ is the mixture dynamic viscosity, μ_T is the turbulent dynamic viscosity, P is the pressure, D_{md} is the turbulent dispersion coefficient, $\mathbf{g}$ is the gravity, $\mathbf{F}$ is the additional volume force vector, τ_{Gm} is the sum of the viscous and turbulent stresses, σ_T is the turbulent particle Schmidt number, c_d is the mass fraction of the dispersed phase, ϕ_d is the volume fraction of the dispersed phase, k is the turbulent kinetic energy, m_{dc} is the mass transfer from dispersed to continuous phase, ρ_c and ρ_d are the densities of the continuous and dispersed phase, respectively. For the relative velocity, the slip model homogeneous flow was assumed ($\mathbf{u_{slip}}=0$) and mass transfer between the phases was not taken into account ($m_{dc}=0$). For the turbulent particle Schmidt number (σ_T), the default value (0.35) was used. To track the dispersed phase, the transport equation of the dispersed phase volumetric fraction is used:

$$\frac{\partial\phi_d}{\partial t}+\nabla\cdot(\phi_d\mathbf{u_d})=-\frac{m_{dc}}{\rho_d} \quad (5)$$

where $\mathbf{u_d}$ is the velocity vector of the dispersed phase. The mixture density is estimated as the two phases volumetric mean density, while the mixture viscosity is estimated using the semi-empirical equation proposed by Krieger and Dougherty (Selvakumar & Dhinakaran, 2017). In order to estimate the turbulence dynamic viscosity, as shown in Eq 6, the k-ε turbulence model uses two additional transport equation, Eq 7 and 9. The turbulent kinetic energy (k) and the energy dissipation rate (ε) are introduced as dependent variables (COMSOL Multiphysics ®, 2017).

$$\mu_T=\rho C_\mu\frac{k^2}{\varepsilon} \quad (6)$$

$$\rho\frac{\partial k}{\partial t}+\rho\mathbf{u}\cdot\nabla k=\nabla\cdot\left[\left(\mu+\frac{\mu_T}{\sigma_k}\right)\nabla k\right]+P_k-\rho\varepsilon \quad (7)$$

$$P_k=\mu_T\left\{\nabla\mathbf{u}:\left[\nabla\mathbf{u}+(\nabla\mathbf{u})^T\right]-\frac{2}{3}(\nabla\cdot\mathbf{u})^2\right\}-\frac{2}{3}\rho k\nabla\cdot\mathbf{u} \quad (8)$$

$$\rho\frac{\partial\varepsilon}{\partial t}+\rho\mathbf{u}\cdot\nabla\varepsilon=\nabla\cdot\left[\left(\mu+\frac{\mu_T}{\sigma_\varepsilon}\right)\nabla\varepsilon\right]+C_{\varepsilon1}\frac{\varepsilon}{k}P_k-C_{\varepsilon2}\rho\frac{\varepsilon^2}{k} \quad (9)$$

where P_k is the production term and C_μ, $C_{\varepsilon1}$, $C_{\varepsilon2}$, σ_k and σ_ε are the model dimensionless constants, whose numerical values were recommended by Launder *et al.* (1973) according experimental data as: 0.09, 1.44, 1.92, 1.0 and 1.3, respectively (Wilcox, 1998; COMSOL Multiphysics ®, 2017).

2.1.2 Geometry

The geometries used in the simulation were built in 3D based on the Cox hydraulic flocculator at the water purification plant in Viterbo, Colombia. Figure 1 shows the 3D geometry used in the simulations for the original design. The studied unit consists of 6 squared horizontal section compartments with an inverted pyramid bottom (chute), as shown in figures 2 and 3. The flocculator chambers main dimensions values are shown in table 1. The b_2 parameter corresponds to the lower side length of the inverted pyramid bottom, which corresponds to the area where the drainage tubes would be installed vertically downwards. The water input window was supposed to be completely submerged. The height of this window corresponds to the crest height of the design volumetric inflow through a rectangular weir of 0.5 m width.

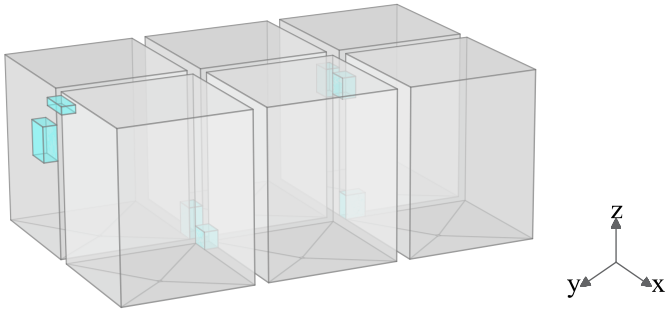

Fig. 1: 3D geometry of the Cox hydraulic flocculator original design used in the CFD simulations. The cyan blocks represent the passages.

Table 1: Main dimensions of the flocculation chambers

Parameter	Value	Units
Number of chambers	6	-
H_1	2.4	m
H_2	0.0925	m
w_t	0.2	m
b_1	1.9	m
b_2	0.0508	m
β	6	deegres

The windows are expected to have a high impact on the flocculation performance, since the highest velocity gradients are generated there. Therefore, in order to evaluate the fluid flow behavior, the windows number and location were modified in this research. The windows horizontal position (on the x axis) were changed, an alternately and an aligned arrangement were implemented as is shown in the figure 2a and 2b. A number of 1 and 2 windows between chambers were also investigated, as shown in figures 3a and 3b. The calculation of the windows area was performed so that in both cases the obtained mean velocity gradient decrease between chambers would be the same, taking as basis the design volumetric input. The areas were estimated using the equations indicated by Lozano-Rivas & Lozano-Bravo (2015). The dimensions of the windows are shown in table 2. In the case where 2 windows were used, both windows were implemented using the same dimensions. The second window was located above the first, separated by a distance equal to half of the height of each pair of windows. This configuration allows having a proportional separation between them (reducing the design degrees of freedom), without compromising structure stability. Only one input and output window to the flocculator domain were used in all cases. The windows located on top of chambers are 0.25 m away from the surface, with the exception of the input and output windows which are at 0.051 m and 0.51 m, respectively. Additionally, the windows at the bottom are just above the chute.

The boundary conditions used through the geometry were: 1. No slip wall, on the flocculators windows and chambers walls. 2. Slip wall, on water surface (where the water is supposed to be in contact with air). 3. Inlet flow, in the flocculator input window. 4. Output atmospheric pressure, in the output channel. From preliminary simulations, it was noticed that the output condition has a considerable effect on the nearby fluid flow. Then, a long output channel was installed and the output results variables were taken at the channel cross section located 0.2 m from the last chamber and the output channel conjunction. Initially, the fluid in the system domain does not contain dispersed phase. The gravity force was also applied through the whole geometry domain in the -z direction (see Fig. 3).

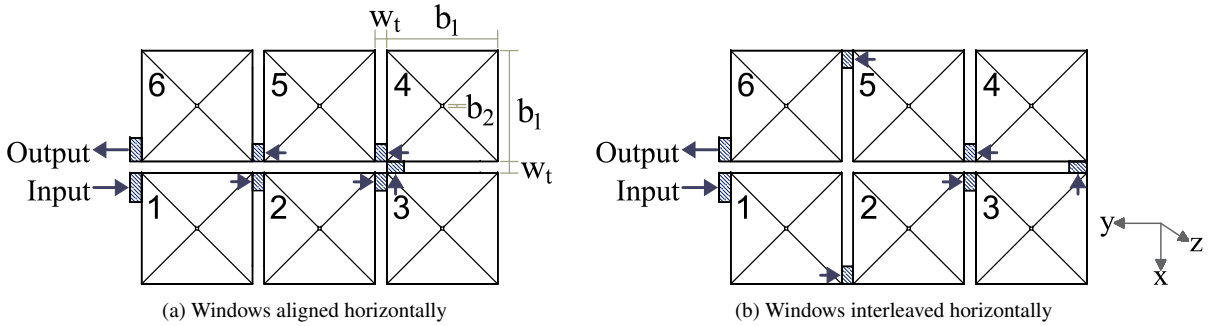

(a) Windows aligned horizontally (b) Windows interleaved horizontally

Fig. 2: Plant view from the top of the Cox hydraulic flocculator. Location of the windows: (a) Windows aligned horizontally and (b) Windows interleaved horizontally. The blue discontinuous diagonal lines represent the flocculator passages.

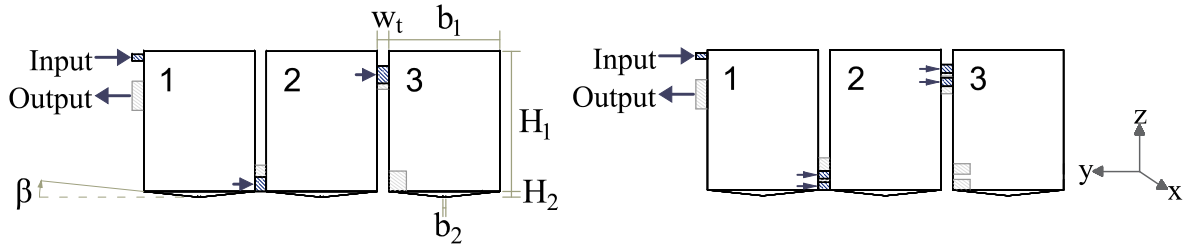

(a) 1 window (b) 2 windows

Fig. 3: Transversal view of the Cox hydraulic flocculator. Number of windows between chambers: (a) 1, (b) 2. The blue discontinuous diagonal lines represent the flocculator passages, while the gray diagonal lines indicate the passages of the chambers located behind the chambers shown in the view.

2.1.3 Simulation parameters

In order to track the injected dispersed phase for the tracer test, dynamic simulations were performed. Table 3 shows the parameters and the properties of each phase in the simulations. The continuous and dispersed phases properties correspond to water and a salt (Sodium chloride), respectively. For the sake of simplicity, it was assumed that the salt is only one species in water. To introduce the dispersed phase, a single square pulse of 1 s width was used on the flocculator input. During which the volumetric fraction of the dispersed phase in the inflow was set as 0.1. In order to evaluate different conditions, two different input flow rates were evaluated. Besides the input flow, two geometric parameters (the windows number and location) were also taken into account for the flocculator assessment. Table 4 summarizes the conditions under which all the cases were carried out.

2.1.4 Numerical methods

The system equations were solved by the finite element method in COMSOL Multiphysics® with GMRES iterative solver and an absolute error tolerance of $5x10^{-4}$. For the chambers, a triangular mesh recommended for fluid dynamics and defined as fine with element size between O(0.0316) < h < O(0.167) m. As higher velocity gradients are expected around the passages between the chambers, a triangular mesh defined as extra fine with O(0.00474) < h < O(0.0727) m was used on these. A number of 3 and 2 boundary layers were also implemented at chambers and conducts walls, respectively. This configuration is aligned with the different meshing of the chambers and passages, finer at the passages, in order to avoid high simulation time. The number of elements and the average element quality used in each case are shown in table 4. The mesh used

Table 2: Main dimensions of the flocculator windows when 1 and 2 windows are used between chambers.

Passages between chambers	Window vertical location	Number of windows between chambers		Width (m)	$\overline{G}$ design* (s^{-1})
		1	2		
		Heigh (m)			
input	upward	0.1094	0.1094	0.5	89.83
1 – 2	downward	0.25	0.13	0.3	59.14
2 – 3	upward	0.3	0.15	0.3	42.90
3 – 4	downward	0.35	0.18	0.3	32.80
4 – 5	upward	0.4	0.2	0.3	26.06
5 – 6	downward	0.45	0.22	0.3	21.32
output	upward	0.5	0.5	0.4	10.64

* The mean theoretical velocity gradient ($\overline{G}$) for the input was calculated for a weir (whose surface is open to the atmosphere), while for the remaining windows, the $\overline{G}$ was estimated as for a submerged orifice. In both cases, Eq.10 was used.

Table 3: Properties and input flows used in the simulations

Parameters		Value		Units
		Continuous P.	Dispersed P.	
Density		999.62	$2.17x10^{3}$	kg/m^3
Dynamic viscosity		$1.01x10^{-3}$	–	Pa·s
Particle diameter		–	$1x10^{-3}$	m
Inlet volumetric fraction		–	0.1	1
Injection time		–	1	s
Volumetric inflow	Design	0.03184		m^3/s
	Operation	0.01377		m^3/s
Gravity		9.81		m/s^2

for the geometry of the flocculator original design is shown in the figure 4. In order to develop the fluid flow through the geometry, for each configuration a preliminary simulation with no dispersed phase was executed for a total time of 2000 s. The last step time of these preliminary simulations was used as initial condition in the simulations where the dispersed phase was tracked, those were performed for times between 10000 and 12000 s, for the cases where the design and operation inlet flow were employed, respectively. Small time steps of 1 s were taken in the first 50 s, as initially the tracer concentration in the first chamber changes drastically. Subsequently, larger time steps were taken (between 20 and 50 s).

2.2 *System performance indexes*

2.2.1 *Velocity gradient*

The velocity gradient is used in flocculation to characterize the mixing degree. Traditionally, this parameter is estimated as an average value, due to its simple calculation (Bridgeman *et al.*, 2009). In a Cox hydraulic flocculator the mean velocity gradient ($\overline{G}$) can be estimated considering each window as a rectangular submerged orifice, as shown in Eq 10 (Arboleda-Valencia, 2000).

$$\overline{G} = \sqrt{\frac{f v^3}{R_h \nu}} \tag{10}$$

Where f is the Darcy friction factor, v is the fluid mean velocity perpendicular to the window, R_h is the hydraulic radius and ν is the kinematic viscosity. However, the flocs are not subjected to this single average velocity gradient, since these are not uniform through the system volume. By means of the local velocity gradient (G_L), the effect of the turbulence in specific zones on the floc formation can be estimated. The local velocity gradient is estimated as follows (Bridgeman *et al.*, 2009):

$$G_L = \sqrt{\frac{\varepsilon}{\nu}} \tag{11}$$

Table 4: Flocculation conditions and meshes used in the cases evaluated through the simulations

Case	1	2	3	4	5	6
Volumetric inflow	operation	design	operation	design	design	design
Windows horizontal location	aligned	aligned	interleaved	interleaved	aligned	interleaved
Number of windows beetween chambers	1	1	1	1	2	2
Number of elements	517,153	517,153	519,497	519,497	518,568	520,456
Average element quality	0.6458	0.6458	0.644	0.644	0.6447	0.6424

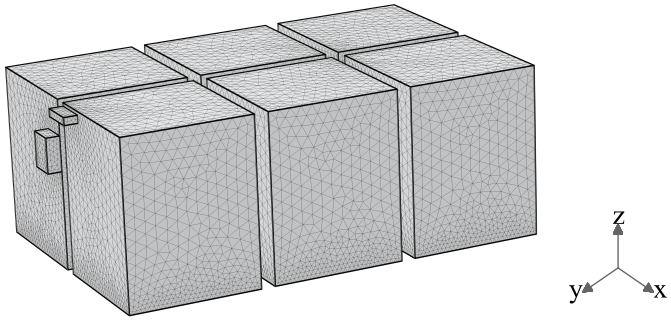

Fig. 4: Mesh used in the CFD simulations for the hydraulic flocculator original design.

The ε value is calculated from the κ-ε turbulence model in each node inside the system domain. The G_L distribution is very valuable to asses the flocculation performance since it controls particle suspension, distribution, coalescence and floc breakage (Essemiani & de Traversay, 2002). As performance indicator, the 95th percentile of the normalized G distribution proposed by Haarhoff & van der Walt (2001) was also analyzed. This indicator indicates the G_L value that is only exceeded in 5% of the total flocculator volume.

2.2.2 *Residence time distribution*

The theoretical hydraulic residence time was calculated using Eq 12, as the ratio between the entire flocculator volume (V) and the volumetric input flow (Q). The theoretical hydraulic residence time per chamber was also calculated by dividing the whole system theoretical hydraulic residence time between the number of chambers.

$$t_t = \frac{V}{Q} \tag{12}$$

A tracer study allows estimating the residence time distribution, from which is possible to identify the flow defects as the stagnant zones and bypassing flow (Fogler, 2008). As representation of the residence time distribution, the $E(t)$ function is used. This function is a measure of the bulk flow patterns in a vessel (Bridgeman *et al*., 2009) and is calculated based on the tracer concentrations taken over time, as follows:

$$E(t) = \frac{\mathrm{C(t)}}{\int_0^\infty \mathrm{C(t)\,dt}} \tag{13}$$

where $C(\mathrm{t})$ is a concentration measure of the tracer at the measurement point as function of time. The mean residence time can be then estimated as:

$$t_m = \int_0^\infty tE(t)\,dt \tag{14}$$

In the last eq, t_m is the mean hydraulic residence time and t is the time since addition of tracer. The integration in Eq 13 was calculated using the software OriginPro 8, by means of numerical integration approaches as the trapezoidal rule, good approximations can also be obtained.

3 Results and discussion

Through the estimation of the local velocity gradients and the hydraulic residence time for each case, the variables as flow velocities, energy dissipation rate and tracer concentration were exported to Microsoft Excel (according to table 4). The simulation performed to obtain the initial flow conditions, required a computation time approximately of 5 h for the cases 2, 4, 5 and 6, while it took 12 h for the cases 1 and 3. Additionally, the final simulations in which the tracer particles were tracked required a computation time of around 40 h for the cases 1 and 3 and between 10 h and 15 h for the remaining cases. All the simulation were compiled in an Intel® Core™ i7 – 7700 3.60 GHz processor and 8 GB of RAM.

3.1 Flow velocity

Figure 5 shows horizontal cutting planes of the flow velocity magnitudes for the case 2 at different heights, and Figure 6 shows the velocity magnitude isocontours in the chambers for the case 2. Both figures show how in each chamber the flow enters throughout the passages with a relatively high velocity and then crash against the wall in front of the inlet window, were the velocity is reduced (see Fig 6d). The velocity vectors in the figure 5 seems to follow a recirculation pattern, showing the existence of swirls inside the chambers. The probability of collision between the flocs can be increased by changes in the flow velocity. The swirls can generate changes in the radial and axial velocities and therefore generate adequate conditions for the flocs agglutination (**?**).

The lowest velocity magnitudes are observed mainly in the center of these swirls and in some of the chamber corners where velocity lower than 0.5 m/s are obtained (for case 2). These minimum velocity magnitudes and the velocity vectors orientation show the existence of stagnant zones in some of these corners (as the upper right corner of the chamber 4 in Fig. 5). The stagnant zones can result in the floc sedimentation and reduces the unit effective volume, which generate that the residence time of some particles in the flocculator decreases. The existence of stagnant zones around these areas (tank corners) has also been reported in others studies, where although others flocculation unit types where evaluated, rectangular cross section tanks were also employed (Vadasarukkai *et al*., 2011; Bridgeman *et al*., 2010). Mohammadighavam *et al*. (2016) for example, could observe stagnant zones at the corners between the baffles and the walls in a horizontal baffled flocculator. Bridgeman *et al*. (2010) compared the hydrodynamic performance of a stirred pilot flocculation tank using two vessels a square and a cylindrical tank using CFD. The cylindrical tank showed a better flow distribution while stagnant zones were not found within this, unlike the square shaped tank where stagnant zones were observed in the tank corners. Therefore, an improvement in the hydrodynamic performance of the Cox flocculators can be expected by implementing cylindrical chambers instead of rectangular since sedimentation undesired could be avoid. Although the construction of the flocculation chambers and passages could not be straightforward and corresponds to a mayor modification to the existing plant.

Figure 7 shows the flow stream lines obtained for the cases 1, 2 and 4. In these figures the

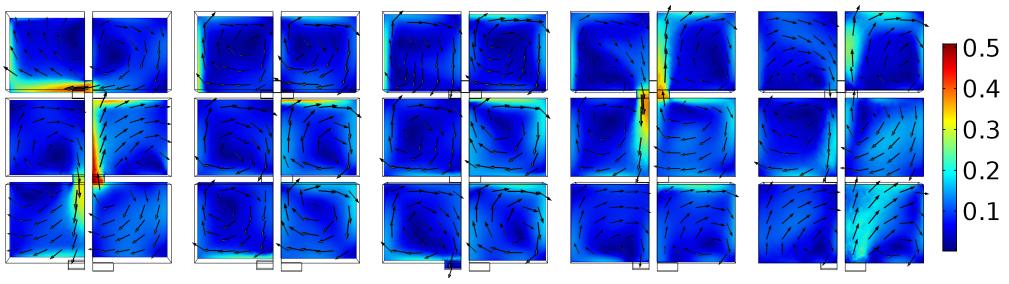

(a) z= 0.2 m (b) z= 0.7 m (c) z= 1.4 m (d) z= 1.9 m (e) z= 2.2 m

Fig. 5: Views from the top of the flow velocity magnitudes horizontal plans at different heights in the z axis for the case 2. Heights in the z axis: (a) 0.2 m, (b) 0.7 m, (c) 1.4 m, (d) 1.9 m and (e) 2.2 m. The velocity magnitudes are in m/s and the black arrows represent the velocity vectors.

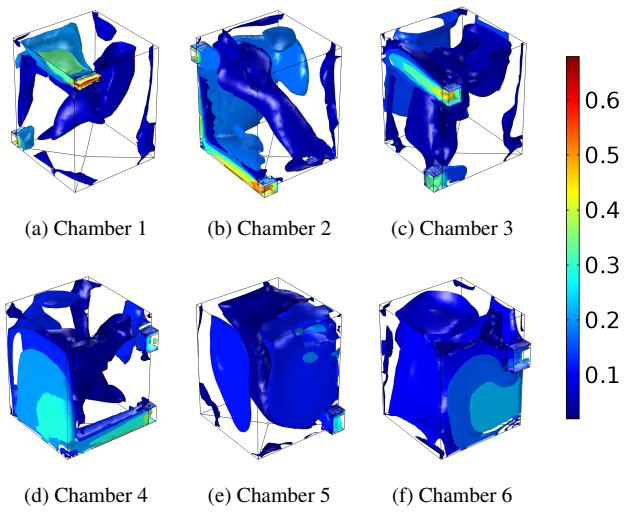

(a) Chamber 1 (b) Chamber 2 (c) Chamber 3

(d) Chamber 4 (e) Chamber 5 (f) Chamber 6

Fig. 6: Velocity magnitudes obtained in each chamber for the case 2. Chambers: (a) 1, (b) 2, (c) 3, (d) 4, (e) 5 and (f) 6. The velocity magnitudes are in m/s.

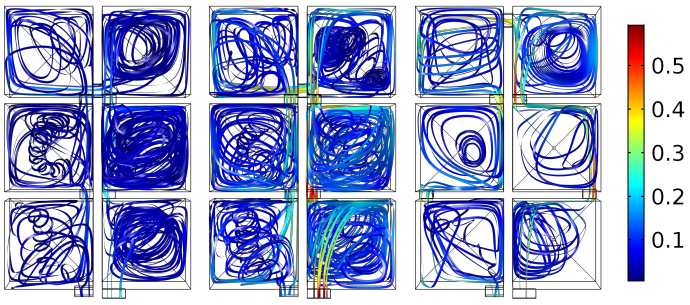

(a) Case 1 (b) Case 2 (c) Case 4

Fig. 7: Plant view from the top of the stream lines in: (a) case 1 (b) case 2 and (c) case 4. The flow lines color represents the flow velocity in m/s.

flow recirculation patterns can also be seen in the focculators chambers. After reaching the steady state, is possible to observe these similar flow behavior in all the cases studied. At the cases where the windows are interleaved (cases 4 and 6), was possible to see in some chambers how a portion of the stream lines after getting into the chamber and crashing against the wall, do not join the whirl. Instead these go directly to the outlet window towards the next chamber (bypassing flow). Due to the bypassing flow a portion of the flow do not go through the entire volume available at the chambers.

Figures 8 and 9 show the mean and the maximum flow velocities obtained for each passage and chamber, respectively. The dashed lines in these figures represent the mean flow velocity needed in each window to obtain the theoretical mean velocity gradients shown in table 2. Since the used wall condition fixes the velocity of the flow at the wall to zero, the minimum velocities were not evaluated. In the cases 5 and 6 two windows between chambers were implemented, hence for these cases a velocity for each window is shown (referred to as upper and lower). The figure 8a shows the mean velocities through the windows. Due to the lower inlet flow

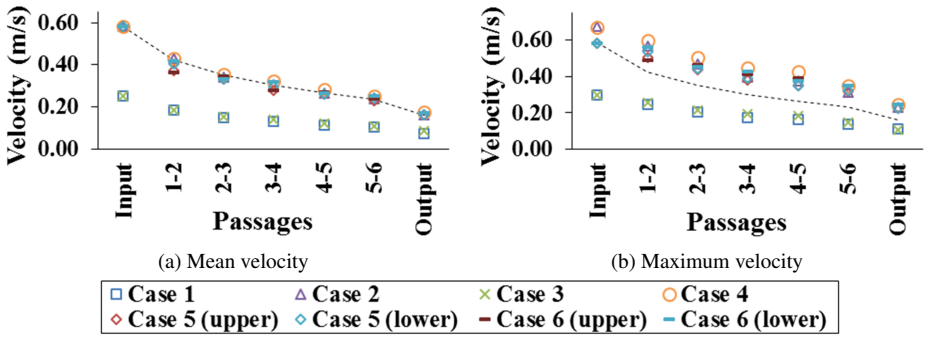

Fig. 8: Velocity magnitudes in the flocculator passages: (a) mean velocities and (b) maximum velocities. The velocity magnitudes are in m/s and the dashed black line represents the theoretical velocities (consistent with the Eq. 10).

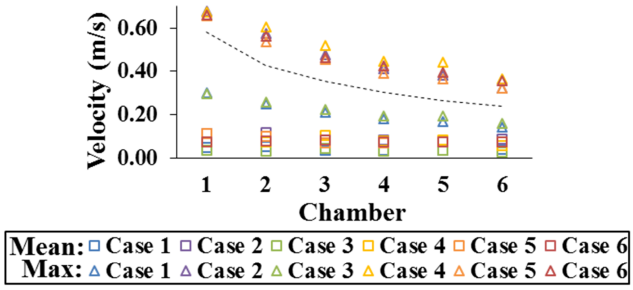

Fig. 9: Mean and maximum velocity magnitudes in the flocculator chambers. The velocity magnitudes are in m/s and the dashed black line represents the passages theoretical velocities (consistent with the Eq. 10).

for the cases 1 and 3, those present an appreciable difference with respect to the theoretical value. As shown in the figure 8b, for the cases 1 and 3 the maximum velocities are still not high enough to reach the theoretical velocities. In the other cases, the theoretical velocity is surpassed between 20 and up to 60%. Where the case 4 presents the highest velocity values while the case 5 shows the lowest maximum velocities, and thus is the closest to the theoretical velocities. The maximum velocities in the chamber are also higher than the mean the theoretical velocities at the corresponding window. This is expected due to velocity profile created by the wall boundary condition, where the flow velocity leaving the window is the lowest adjacent to the walls and the highest at the sine of the fluid. As is shown in the figure 6, the maximum velocities are obtained mainly around the inlet area due to the lower cross section of the windows. Pérez-Parra (2006) suggests that in order to avoid the flocs rupture and sedimentation in the flocculation unit, the mean velocity should be lower than 0.6 m/s and higher than 0.1 m/s, respectively. In all the cases, the mean velocity in all the chambers is lower than 0.1 m/s, with the exception of the chamber 1 in some cases (on the other hand, velocities higher than 0.6 m/s are only obtained in the cases 2, 4, 5, and 6 at the chamber 1. This indicates that for all cases, the flocs sedimentation should be occurring in some proportion in the flocculation chambers). Then, the flow velocity only seem to be higher enough to break the floc in the zones around the inlet window at the chamber 1 in all the cases with the exception of cases 1 and 3, were low velocities were obtained.

3.2 *Velocity gradient*

In order to get a general insight of the velocity gradient, the mean gradients per chamber and global average, are compared with the theoretical gradients in table 5. Due to the lower inflow in the cases 1 and 3, lower gradients than the required are obtained. These low gradients can cause the non-floc formation and

Table 5: Average local gradients per passage

Passages	Theoretical	Average local gradient (s^{-1})					
		Case 1	Case 2	Case 3	Case 4	Case 5	Case 6
1 – 2	59.14	21.97	77.87	22.96	80.11	79.12	89.22
2 – 3	42.9	13.23	49.19	20.82	74.69	47.53	44.23
3 – 4	32.8	7.81	7.49	15.15	53.09	30.04	52.67
4 – 5	26.06	12.2	43.26	13.34	50.45	43.36	76.61
5 – 6	21.32	6.15	21.4	7.66	24.13	25.17	31.21
Output	10.64	5.26	19.28	12.04	33.34	17.68	19.46
Global	32.14	11.1	36.41	15.33	52.63	40.48	52.23

sedimentation in the chambers, causing an increasing in the water turbidity and therefore a decrease in the unit efficiency. In the other cases, with the design inflow, mainly higher gradients than the theoretical were obtained (with the exception of the passage 3 – 4 in the cases 2 and 5). Although in the cases 4 and 6 the design inflow was employed, a higher difference with the theoretical value in comparison with the case 1 and 3 was observed. The cases 2 and 5 (in which the aligned window arrangement was implemented) show the lowest difference with the theoretical $\overline{G}$ value. Among them, the case 5 showed the smallest (where two windows were used). Differences on the velocity gradient values higher than 35% over theoretical values were only observed in the passages 4 – 5 and in the system output.

According to the 0330 Colombian Resolution of 2017 "Technical regulation for the drinking water and basic sanitation sector– RAS", the gradients should be between 70 and 10 s^{-1} to guarantee an adequate flocculation, in hydraulic flocculation systems. Only gradients lower than 10 s^{-1} are seen in the last passages of the cases with the lower inflow (cases 1 and 3), while gradients higher than 70 s^{-1} were mainly obtained in the first and second passage of the case 4 and only in the first in the cases 2, 5 and 6. This implies that in the later passages the flocculation conditions are not the optimal and flocs disruption can take place inside these sections. The $\overline{G}$ values in the remaining passages are within the recommended range.

In order to promote floc growth and to avoid their destruction, the gradient values should also be decreasing as it is shown in theoretical data in table 5. Thus, more collisions are required at the beginning of the process to increase the flocs size, while at the end, less collisions are preferred to avoid breaking. In cases 1, 2, 5 and 6 there is a reduction in the mean G value until the step 3–4, which is followed by a sudden gradient increase in the step 4 – 5 (which can cause the breaking of previous formed flocs). This issue is not seen in the cases 3 and 4 in which the windows horizontal position was alternated. In these two cases, the gradient raising occurs in the exit passage. This gradient decrease issue is related with the location of this passage, which in order to connect passages 3 and 4 is located in a different way in comparison with the other passages. However, these results indicate that a configuration with a better hydrodynamic performance could be achieved by modifying the window location in the troubled passage (in this case the passage 3 – 4).

In the figure 10 the G_L magnitudes through the flocculation chambers and passages for the cases 1, 2 and 5 are shown. In figure 10 n and p, in which 2 windows were used, it can be seen that slightly higher gradients values are obtained in the lower window at the downward passages. In accordance with the velocity magnitudes, higher gradients in each chamber are obtained close to the input passages and in the front wall where the fluid hits (see figure 10 j and l). The gradient increases again around the output window due to the narrow area, while the G_L values seem to be relatively low in the remaining areas of each tank. This results show a high spatial variation of G_L in the flocculation chambers. This is a problem since the flocs can be subjected to zones with high and low velocity gradients inside the same chamber. The spatial non-uniformity of ε and therefore of G_L in hydraulic and mechanical flocculators has also been reported by others authors (Haarhoff & van der Walt, 2001; Bridgeman *et al*., 2010; Vadasarukkai *et al*., 2011; Mohammadighavam *et al*., 2016; **?**).

In figure 11, the local gradient cumulative occurrence (G_L) for different passages for cases 4 and 5 are shown. This quantity indicates the maximum G_L value obtained for an accumulated percentage

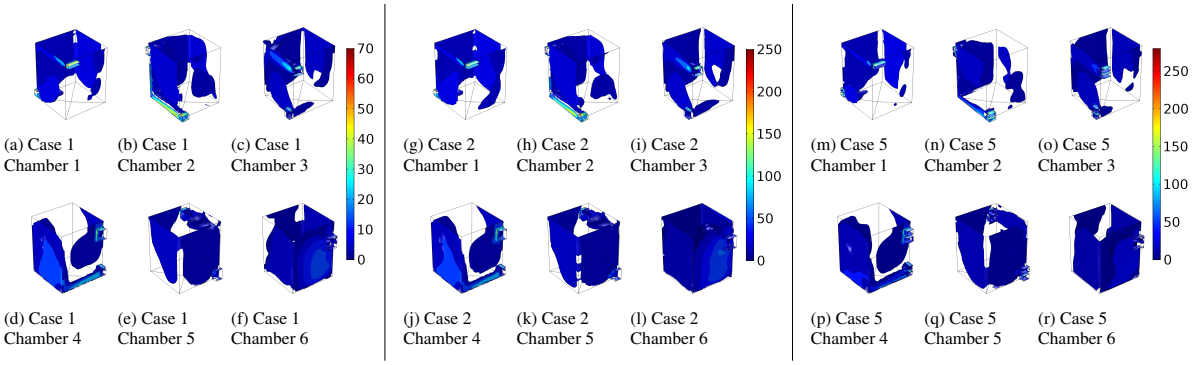

Fig. 10: Local gradient magnitudes obtained in each chamber for the cases 1, 2 and 5. Cases−chambers: (a) 1 – 1, (b) 1 – 2, (c) 1 – 3, (d) 1 – 4, (e) 1 – 5, (f) 1 – 6, (g) 2 – 1, (h) 2 – 2, (i) 2 – 3, (j) 2 – 4, (k) 2 – 5, (l) 2 – 6, (m) 5 – 1, (n) 5 – 2, (o) 5 – 3, (p) 5 – 4, (q) 5 – 5 and (r) 5 – 6. The local gradient magnitudes are in s^{-1}.

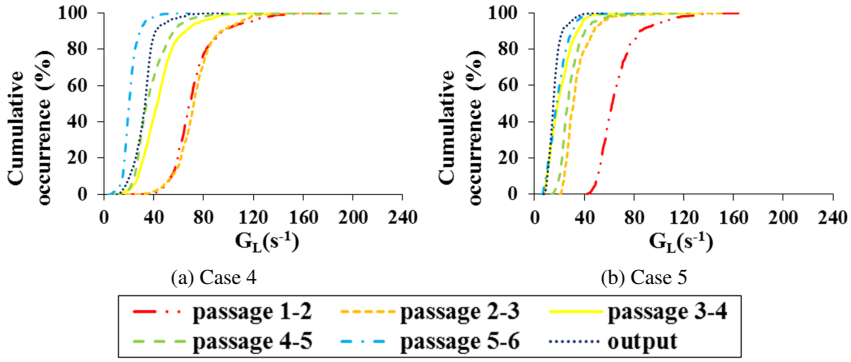

Fig. 11: Distribution of the local velocity gradient per each chamber: (a) case 4 and (b) case 5.

of volume in a passage. In case 4, the gradient distribution is adequate until the exit passage unlike case 5 where there is an abrupt increase in the passage 4−5. In case 5, the highest gradients are obtained in the passage 1−2 where gradients between 129.1 and 168.8 s^{-1} are obtained in the 1% of the volume. For case 4, G_L values from 138.7 to 190.2 s^{-1} were obtained for the 1% of volume of the first step. However, in this case the highest gradients were obtained at the passage 4 – 5, with a G_L range between 86.72 and 239.8 s^{-1}. Which shows a high G_L variability at this passage. Vadasarukkai *et al*. (2011) reported a the G_L distribution for each tank of a tapered hydraulic flocculator. They found higher maximum G_L values at the high turbulence zones, since for the first tank in 1% of the tank volume G_L values from 254.8 and up to 1,230.5 s^{-1} were reported. This indicates that the large variability generated by high values of G at turbulence zones is an issue in most of hydraulic flocculators.

In order to present the G_L distribution in a more simplified way, in tables 6 and 7 the obtained G_L value are shown for 25, 50 and 95% of accumulated frequency per passage for all the cases. For the cases where two windows were used, both windows distribution were estimated as one. In cases 2 and 5, 50% of the volume in the passage 1 – 2 presents gradients of 62 s^{-1} or lower, while in cases 4 and 6 the 50% of the volume presents gradients up to 73 s^{-1}. These high gradients favor the flocculation process during the initial period of floc formation.

Table 6: Percentiles of the local gradients values per passage for the cases 1, 2 and 3

Passages	Case 1			Case 2			Case 3		
	25%	50%	95%	25%	50%	95%	25%	50%	95%
1 – 2	17	22	42	51	62	105	18	20	31
2 – 3	9	10	24	30	35	98	18.2	20.2	30
3 – 4	3.8	5	12	12.5	18	42	9.7	12	21
4 – 5	7.7	8.8	15	24	30	55	5.9	10.7	16
5 – 6	3.2	4.5	10	13	16	36	5.8	6.6	11
Output	3.9	4.6	9	13	16	32	9.7	10.5	18

Table 7: Percentiles of the local gradients values per passage for the cases 4, 5 and 6

Passages	Case 4			Case 5			Case 6		
	25%	50%	95%	25%	50%	95%	25%	50%	95%
1 – 2	62	71	115	57	63	104.2	65	73	115
2 – 3	61.7	70	110	28	32	54	26	30	84.9
3 – 4	34.8	43	75	13	15	38.4	35	40.8	70.2
4 – 5	28	33	63	22	25	45.8	49	55.2	84
5 – 6	17.8	19.5	32.5	13	15	33.8	20.4	24.9	42
Output	28	32.8	50	13	14.8	29	13.6	16	27

From other side, for cases 1 and 3 (lower volumetric inflow), the G_L value for all the percentiles are lower than their corresponding theoretical value. This means that even in the highest turbulent zones, the floc is submitted to a G_L lower than the required. Thus, a poor flocs approach and agglutination is expected. For the remaining cases, G values significantly higher than theoretical values were obtained for the 95% percentile. For cases 2 and 5, lower or closest G_L values to the theoretical were obtained for the 25 and 50 percentile, unlike the cases 4 and 6 were the highest values were obtained. Thus, the cases with the interleaved arrangement, showed the highest G_L percentiles values, and therefore these are the most distant to the required theoretical value, with a mean G_L error of 85.7 and 67.4% for the cases 4 and 6, respectively. When comparing the performance of the cases with 1 window per chamber (i.e. cases 2 and 4) with the cases with 2 windows (cases 5 and 6), an improvement in the G_L values was observed when using 2 windows, since the mean error decreased between 10 and 20%, by employing 2 windows instead of 1. The case 5, where the passages horizontal position was kept alienated and 2 windows were used, showed the G_L percentile values closest to the theoretical, with an error of 42.2%. While for the case 2 a mean error of 52.7% was obtained for the gradient distribution.

The improvement in the G_L distribution obtained by increasing the number of windows could be related to the increase of the contact area between the fluid and the solids walls at the passages and to the wall boundary condition used. The no-slip wall boundary condition fixes the flow velocity to zero, thus the flow velocity increases sharply from zero at the wall to the velocity at the sine of the fluid. Therefore, right at the wall the turbulence is zero and in the close vicinity of the wall the molecular effects become more dominant than the turbulent properties of the flow (Dewan, 2011). Since the passages transversal area was kept constant when the number of windows was increased, the resulting wall/fluid contact area increase could contribute to some extent to control and decrease the flow high turbulences developed in the passages.

In some scenarios, a considerable difference between the values obtained for each percentile in tables 6 and 7 is observed. This implies the existence of some gradient variabilities inside the passages. The difference between the 25 and 50 percentiles for case 4, 5 and 6 are around 8 and 20%, respectively. This indicates that the changes are small and have almost uniform gradients. However, higher differences are obtained when comparing the 50 and 95 percentile, where differences between 36 and 70% are estimated.

3.3 Residence time distribution

The theoretical hydraulic residence time was used as basis for comparing the residence times estimated from the CFD simulations. Table 8 shows the theoretical hydraulic residence times calculated for the whole flocculation system and for each flocculation chamber employing a flocculation unit total useful volume of 48.74 m^3. Two different hydraulic residence times are also obtained for each one of these since two input flows were evaluated.

In order to analyze the particles residence time inside the system, a tracer was injected and subsequently tracked. Figure 12 shows the tracer volume fraction through the flocculation chambers at different times for the case 2. Taking into account that the relative accuracy (eps) of the CFD software is approximately $2.22x10^{-16}$, only tracer volume fractions larger than 10^{-20} were considered, since values of an order of magnitude of 10^{-20} are small enough to be considered as zero (COMSOL Multiphysics ®, 2017). The figures show as after 1 s, all the tracer is already inside the first chamber (Figure 12a). The tracer is then dragged by the fluid flow through the chamber volume and get into the next one (Figure 12b and c). A similar behavior is repeated sequentially in all the chambers until finally all the tracer reach the exit passage at the last chamber. However, as all the particles do not leave a certain chamber at the same time, a considerable variability in the residence time is anticipated. The variability of the residence time is also expected to be increasing chamber to chamber, due to the spreading in the previous chambers. A similar tracer concentration distribution is also obtained in the other cases, aside from the cases 1 and 3 were in order that the tracer particles leave the flocculation unit domain, higher hydraulic residence times are required.

The table 8 shows the mean global hydraulic residence time (t_m), its error and standard deviation (SD) obtained using the tracer mean concentrations profiles through the last flocculator chamber. The global residence time error is calculated taking as basis the respective theoretical hydraulic residence time (t_t). It can be seen that although the global t_m increase for the cases where the lowest inflow is used (cases 1 and 3), the error with the theoretical value is lower in comparison with the cases where the highest input flow was used (cases 2 and 4). Vadasarukkai *et al.* (2011) employed a particle track model to evaluate the residence time distribution in a three-stage tapered hydraulic flocculation unit. A considerable difference between the mean residence time and the theoretical residence time was observed. They reported a t_t and t_m of 154 and 107.9 min, respectively. This results in an error of 30%, which it is slightly higher than the maximum difference found here. However, they reported a considerably lower standard deviation (6.82 min) in comparison with the observed in this study.

On the other hand, the cases 1, 2 and 5, where the windows are located aligned, present the lowest difference with basis to t_t with errors lower than 5%. In the remaining cases, where the windows are interleaved, errors highest than 14% and up to 26% were obtained. An increase in the global t_m between 10% and 17% was also observed by modifying only the windows position from aligned to interleaved. The windows interleaved arrangement, is supposed to make the water to travel a longer path in each chamber until reach the passage window to the next chamber, thus, higher t_m can be expected for this arrangement. With respect to the number of windows, a less considerable difference was observed between the two arrangements evaluated. When 2 windows are used instead of 1, the error rate is reduced slightly

Table 8: Theoretical hydraulic residence times, mean hydraulic residence times, error rates, standard deviations (SD) and coefficients of variation (CV) obtained for the flocculators cases. D and O represent the design and operation inflow, respectively.

Cases		1	2	3	4	5	6
Volumetric inflow		O	D	O	D	D	D
t_t (min)	Global	58.99	25.51	58.99	25.51	25.51	25.51
	Chamber	9.83	4.25	9.83	4.25	4.25	4.25
Global t_m (min)		61.23	26.78	67.47	32.25	26.69	31.10
Error rate (%)		3.80	4.98	14.39	26.44	4.64	21.93
SD (min)		24.92	11.23	29.89	14.95	10.97	13.50
CV (%)		40.7	41.95	44.3	46.37	41.09	43.4

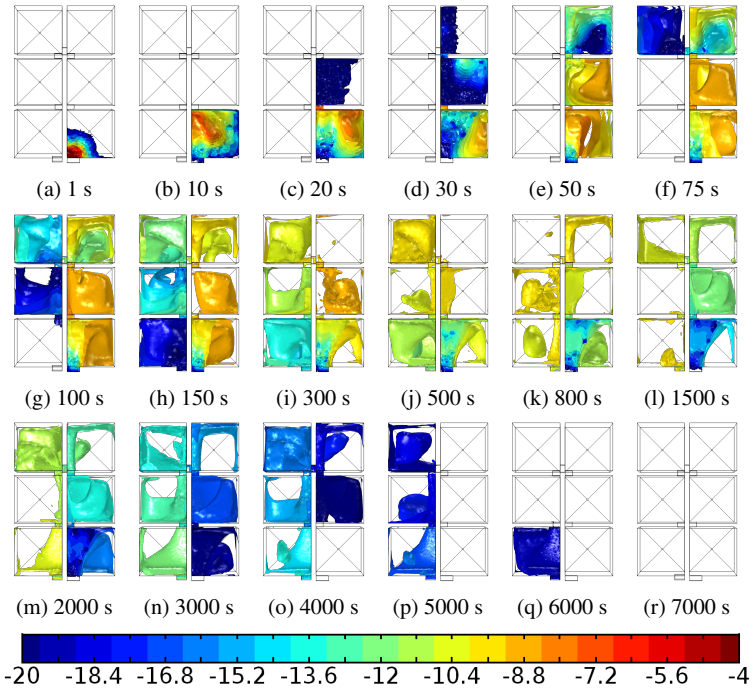

Fig. 12: Plant view from the top of the logarithm of tracer volume fraction ($log_{10}(\phi_d)$) as a function of time for the case 2. time: (a) 1 s, (b) 10 s, (c) 20 s, (d) 30 s, (e) 45 s, (f) 75 s, (g) 100 s, (h) 150 s, (i) 300 s, (j) 500 s, (k) 800 s, (l) 1500 s, (m) 2000 s, (n) 3000 s, (o) 4000 s, (p) 5000 s, (q) 6000 s, (r) 7000 s.

when comparing the cases 2 and 5 and a little more pronounced when comparing cases 4 and 6 (with a decreasing of 0.34% and 4.51%, respectively). A decrease in the global t_m of 0.33% and 3.5% (between the cases 2−5 and 4−6, respectively) was also obtained by only increasing the number of windows from 1 to 2. These global results indicate that the windows horizontal location has considerable influence on the global hydraulic residence time, while the number of windows between chambers has little effect on the global hydraulic residence time as long as the passage area between chambers is kept constant.

The table 8 also shows the coefficient of variation (CV) of each case, aimed to measure the dispersion, understood as the relation between deviation and median. The highest coefficient appears in case 4, which means that the hydraulic residence time in this case has higher variation (its residence time is higher than the theoretical). Therefore, the presence of hydraulic problems as stagnant zones are expected for this case, mainly in the chambers corners where the flow velocity is close to zero. On the other side, it is appreciated in case 1 the lowest variation coefficient (followed of case 5), although it evinces the presence of dead zones. In these two cases, there is a better flow distribution in the chambers even though the CV value is still significant. In general, the variation coefficients shown in table 8 are really high, which implicates significant hydraulic issues. These can be caused mainly by the presence of dead zones, which increases the residence time and hence decreases the efficiency of the flocculation process. It is important to highlight that given the geometry of the systems, great hydraulic issues appear caused by the water stagnation in corners or by the high crashing velocity that the fluid describes at the moment of entering the chamber (which can cause the floc breaking).

In the figure 13a and b are shown the hydraulic residence times (t_m) estimated per chamber with the operational and design volumetric input. The residence times in each chamber can be higher or lower than the theoretical value (which is indicated with a dashed line). This indicates that some particles stay in each chamber longer or shorter time than the required. Therefore, it shows the existence of dead spaces and bypassing flow in some chambers. The

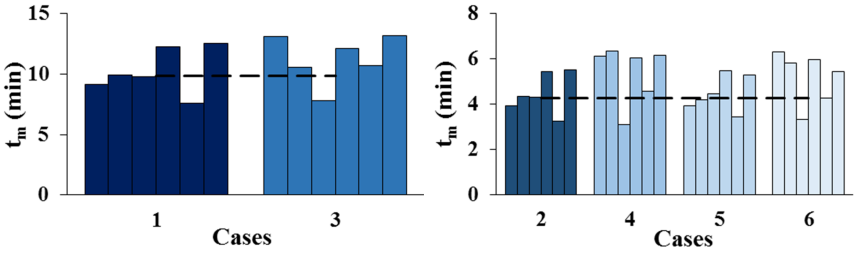

(a) Operation inflow (b) Design inflow

Fig. 13: Mean hydraulic residence time per chamber with a) Operation inflow and b) Design inflow. The 6 bars in each case represent from left to right the chambers 1 to 6 and the dashed lines correspond to the theoretical hydraulic residence time per chamber with both volumetric inflows.

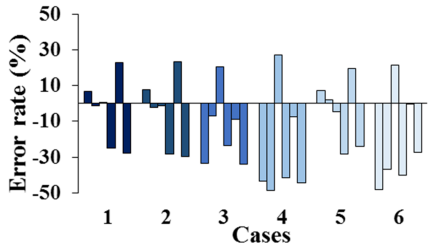

Fig. 14: Error rate of the hydraulic residence time per chamber with basis to the theoretical value. The 6 bars in each case represent from left to right the chambers 1 to 6.

t_m error rate per chamber is also shown in the figure 14, where error rate values highest than the global obtained for each case can be seen. These results indicate that dead spaces and bypassing flow obtained in each chamber compensate each other, allowing obtaining a global t_m closest to the theoretical and therefore a lower global error. However, this means that the time that the flow will be subjected to a certain velocity gradient in each chamber is not supposed to be the same, since in some chambers higher or lower residence times than the appropriate can be achieved. For these reason, a special attention has also been paid to the t_m per chamber. A similar situation was found experimentally by Macías-Quiroga (2016), who used a tracers test to evaluate different designs of an electrocoagulation system. The configuration in which dead zones and bypassing flow were identified simultaneously, also showed the t_m closest to the expected t_t.

The cases 1, 2 and 5, where the windows have been located horizontally alienated, present a similar behavior with respect to the t_m. As is shown in the figure 13a and b, the t_m in the first three chambers is closer to the t_t, with errors lower than 8% (Fig. 14). In this cases the t_m slightly increases from the first until the third chamber. In the chambers 4 and 6, the t_m reaches values more markedly above the theoretical, with errors between 23% and 30%. However, at the chamber 5 the t_m decreases below t_t, where errors between 19% and 23% are achieved. The pronounced difference in the behavior of the t_m between the first three chambers (1 to 3) and the last chambers (4 to 6) in the cases 1, 2 and 3 can be explained by the location of the window 3 – 4. As it is shown in the figure 2a, in order to connect the chambers 3 and 4, this window is located in a different position in comparison with the other windows. The modification of this window location should modify the flow path in the chamber, causing that the hydraulic residence time in the following chambers change. Therefore, it is thought that in order to avoid this increasing in the t_m a better arrangement for the passage between chambers 3 and 4 could be found.

For other side, in cases 3, 4 and 6, in which the windows were located horizontally interleaved, a change in the t_m behavior due to the passage 3 – 4 was

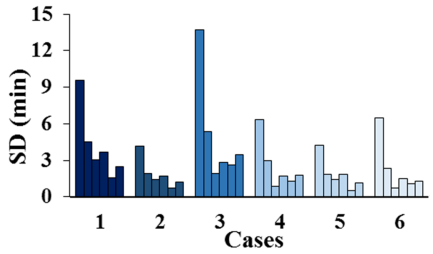

Fig. 15: Standard deviation of the hydraulic residence time per chamber. The 6 bars in each case represent from left to right the chambers 1 to 6.

not observed. As seen in the figure 13b, in comparison with the previous cases, highest t_m per chamber are obtained in cases 4 and 6, mainly in the chambers 1, 2, 4 and 6, where errors from 27% and up to 49% can be obtained. In case 3, the same chambers also presented t_m values above the theoretical but with lower error rates (from 7% until 34%). In these three cases, the t_m in the chamber 3 is lower than t_t with errors between 20% and 27%. The chamber 5 has the lowest error for the cases 4 and 6 (< 8%) while the chambers 2 and 5 present the lowest error in the case 3 (< 9%). There is not a clear similar behavior between the three interleaved window cases. The highest similarities can be seen between the cases 4 and 6, which only differ in the number of windows between chambers. On the other hand, cases 3 and 4, which only differ in the inlet volumetric flow, show a marked difference in the t_m per chambers.

The t_m values obtained per chamber confirm the stated with the t_m global results. The number of chambers has not a significant effect on the hydraulic residence time, while the horizontal location arrangement showed a high effect. The cases 2 and 5 present the best t_m distribution since, the lower difference with t_t and the lower standard deviation are obtained with these arrangements. The interleaved arrangement showed the global and per chamber t_m values more distant from the theoretical values. While the cases with the largest input flow showed the highest standard deviation values.

Conclusions

In this contribution a CFD approach is proposed in order to evaluate and compare the hydrodynamic behavior of a Cox hydraulic flocculator under different geometry and inflow conditions. Through these CFD simulations, it was possible to obtain a better description of the main variables distribution inside the flocculator chambers and passages than conventional approaches.

The simulation results indicate that the inlet flow rate has a high effect on the flocculation performance. When a lower value than the design one was used, higher hydraulic residence times than the theoretical were observed while lower gradients and flow velocities. Due to the rectangular geometry proposed, the presence of stagnant zones in most of the tanks were identificated mainly at the chambers corners. The occurrence of stagnant zones is related with the high values for the residence time coefficient of variation estimated for all the cases, which implicates significant hydraulic issues. The gradient distribution also showed high variance in the flocculation chambers, since high gradients were observed around the windows and close to the wall where the flow crashes. Additionally, low flow velocities and gradients were identificated in the other sections of the chambers, which can lead to the floc sedimentation inside the flocculation chambers.

The horizontal location and quantity of the windows also showed a high effect on the velocity gradient distribution. By modifying the window location from interleaved to aligned and by increasing the number of windows from 1 to 2, it was possible to decrease the global gradient error rate. On the other hand, the number of windows between chambers showed a negligible effect on the hydraulic residence time (as long as the passage area between chambers is kept constant), while the windows horizontal location showed to have a considerable effect on it. By using the aligned windows instead of the interleaved arrangement, it was possible to decrease the global residence time standard deviations, coefficients of variation and error rates (as most of the hydraulic

residence time error rates per chamber). The hydraulic residence time distribution showed a negligible improvement when using 2 windows instead of 1.

In case 5, where the passages horizontal position was kept alienated and 2 windows were used, showed the best G_L and t_m distribution. However, in the aligned arrangement cases (1, 2 and 5) a sudden increase of the G_L distribution values was observed around the step 3 – 4. Since this can induce the previous formed flocs breaking, a new configuration for this problematic step can be proposed in order to obtain a better gradient distribution for case 5, which presented the best hydrodynamic behavior. Through this research, CFD has shown its potential to evaluate different flocculator designs of an unit used in a real water purification plant. This approach eliminated the need to implement modifications to the real structures and employ mean values to characterize the system. Therefore, it was possible to find designs parameters that allow increasing the flocculation unit performance for future implementation.

Nomenclature

b_1	side length of the chamber cross section, m
b_2	side length of the chute drainage cross section, m
$C_{\varepsilon 1}, C_{\varepsilon 2}, C_\mu$	k-ε turbulence model constants, dimensionless
c_d	mass fraction of the dispersed phase, dimensionless
CV	coefficient of variation, dimensionless
D_{md}	turbulent dispersion coefficient, m^2s^{-1}
$E(t)$	fluid exit age distribution, s^{-1}
$\mathbf{F}$	volume force, Nm^{-3}
f	Darcy friction factor, dimensionless
$\overline{G}$	mean velocity gradient, s^{-1}
G_L	local velocity gradient, s^{-1}
$\mathbf{g}$	gravity, ms^{-2}
H_1	height of the chamber upper section, m
H_2	height of the chute, m
h	element size, m
m_{dc}	mass transfer from dispersed to continuous phase, $kgm^{-3}s^{-1}$
P	pressure, Pa
P_k	production term, kg m^{-1} s^{-3}
Q	volumetric flow rate, m^3s^{-1}
R_h	hydraulic radius, m
SD	standard deviation, min
t	time, s or min
t_t	theoretical hydraulic residence time, s
t_m	mean hydraulic residence time, s
$\mathbf{u}$	mixture velocity vector, ms^{-1}
$\mathbf{u_d}$	velocity vector of the dispersed phase, ms^{-1}
$\mathbf{u_{slip}}$	relative velocity between the two phases, ms^{-1}
V	volume, m^3
v	fluid mean velocity perpendicular to the window, ms^{-1}
w_t	wall thickness, m

Greek symbols

β	inclination angle of the chute, deegres
ε	energy dissipation rate per unit mass, m^2s^{-3}
κ	turbulent kinetic energy, m^2s^{-2}
μ	mixture dynamic viscosity, Pa·s
μ_T	turbulent viscosity, Pa·s
ν	fluid kinematic viscosity, m^2s^{-1}
ρ	mixture density, kg m^{-3}
ρ_c	continuous phase density, kg m^{-3}
ρ_d	dispersed phase density, kg m^{-3}
σ_T	turbulent particle Schmidt number, dimensionless
$\sigma_k, \sigma_\varepsilon$	k-ε turbulence model constants , dimensionless
τ_{Gm}	sum of the viscous and turbulent stresses, kg m^{-1} s^{-2}
ϕ_d	volume fraction of the dispersed phase, dimensionless

References

Arboleda-Valencia, J. (2000). *Teoría y Práctica de la Purificación de la Agua*. (3rd ed.). Bogotá, Colombia: McGraw-Hill.

Bratby, J. (2016). *Coagulation and Flocculation in Water and Wastewater Treatment*. (3rd ed.). London, UK: IWA Plushing.

Bridgeman, J., Jefferson, B., & Parsons, S. (2010). The development and application of cfd models for water treatment flocculators. *Advances in Engineering Software 41*, 99 – 109. Civil-Comp Special Issue.

Bridgeman, J., Jefferson, B., & Parsons, S. A. (2009). Computational fluid dynamics modelling

of flocculation in water treatment: A review. *Engineering Applications of Computational Fluid Mechanics 3*, 220–241.

Castellanos, P. (1982). Manual i: teorías. chapter Estudio del comportamiento de un floculador hidráulico de flujo helicoidal. (pp. 264 – 306). Facultad de Ingeniería Civil, Universidad de la Salle, Bogotá, Colombia.

Cheremisinoff, N. P. (2002). *Handbook of Water and Wastewater Treatment Technologies*. USA: Butterworth - Heinemann.

COMSOL Multiphysics ® (2017). CFD module users guide.

Contreras-Andrade, I., Licea-Claveríe, A., Sarmiento-Sánchez, J., Aguilar-Aguirre, M., Quiñonez-Angulo, M., & Picos-Corrales, L. (2015). Synthesis of flocculants based on responsive polymers and its use in solids removal from river water and wastewater. *Revista Mexicana de Ingeniería Química 14*, 415 – 427.

Daigger, G. T. (2011). A practitioner's perspective on the uses and future developments for wastewater treatment modelling. *Water Science and Technology 63*, 516–526.

Dewan, A. (2011). Tackling turbulent flows in engineering. chapter 2: Fluid Turbulence. (pp. 19 – 29). Springer-Verlag Berlin Heidelberg.

Essemiani, K., & de Traversay, C. (2002). Optimisation of the flocculation process using computational fluid dynamics. In *Chemical Water and Wastewater Treatment VII, Proceedings of the 10th Gothenburg Symposium* (pp. 41–50). IWA Publishing.

Fogler, H. S. (2008). *Elementos de Ingeniería de las Reacciones Químicas*. (4th ed.). Mexico: PEARSON Educación.

Haarhoff, J., & van der Walt, J. J. (2001). Towards optimal design parameters for around-the-end hydraulic flocculators. *Journal of Water Supply: Research and Technology - AQUA 50*, 149–159.

Launder, B., Morse, A., Rodi, W., & Spaldiug, D. (1973). The prediction of free shear flows - a comparison of the performance of six turbulence models. In *Proceedings of NASA Conference on Free Shear Flows, Langley* (pp. 361–426). volume 1.

López-Vidal, R., Laines-Canepa, J., Hernández-Barajas, J., & Aparicio-Trápala, M. (2014). Evaluación de almidones de malanga (*colocasia esculenta*) como agentes coadyuvantes en la remoción de turbiedad en procesos de potabilización de agua. *Revista Mexicana de Ingeniería Química 13*, 855 – 863.

Lozano-Rivas, W. A., & Lozano-Bravo, G. (2015). *Potabilización del Agua: Principios de Diseño, Control de Procesos y Laboratorio*. (1st ed.). Bogotá, Colombia: Universidad Piloto de Colombia.

Macías-Quiroga, I. F. (2016). *Optimización de un reactor electroquímico para el desarrollo de procesos de electrocoagulación a escala de planta piloto*. Master's thesis Universidad de Castilla - La Mancha, Ciudad Real, España.

Mohammadighavam, S., Heiderscheidt, E., Marttila, H., & Kløve, B. (2016). Optimization of gravity-driven hydraulic flocculators to treat peat extraction runoff water. *Journal of Irrigation and Drainage Engineering 142*, 04015045AB.

Norton, T., & Sun, D. W. (2006). Computational fluid dynamics (CFD) - an effective and efficient design and analysis tool for the food industry: A review. *Trends in Food Science & Technology 17*, 600 – 620.

Oliveira, D. S., & Teixeira, E. C. (2017). Hydrodynamic characterization and flocculation process in helically coiled tube flocculators: an evaluation through streamlines. *International Journal of Environmental Science and Technology 14*, 2561–2574.

Pan, H., Chen, X., Liang, X., Zhu, L., & Luo, Z. (2016). CFD simulations of gas-liquid-solid flow in fluidized bed reactors - a review. *Powder Technology 299*, 235 – 258.

Pérez-Parra, J. A. (2006). *Manual de Potabilización del Agua*. (3rd ed.). Medellín. Colombia: Facultad de Minas, Universidad Nacional de Colombia.

Raffo-Durán, J., Figueredo-Cardero, A., & Dustet-Mendoza, J. (2014). Características de la hidrodinámica de un biorreactor industrial tipo tanque agitado. *Revista Mexicana de Ingeniería Química 13*, 823 – 839.

Romero-Rojas, J. A. (2006). *Purificación del Agua*. (2nd ed.). Bogotá, Colombia: Escuela Colombiana de Ingeniería.

Selvakumar, R. D., & Dhinakaran, S. (2017). Effective viscosity of nanofluids - a modified krieger-dougherty model based on particle size distribution (PSD) analysis. *Journal of Molecular Liquids 225*, 20 – 27.

Sharma, B. (2007). *Environmental Chemistry*. Krishna Prakashan Media, Delhi, India.

Vadasarukkai, Y. S., Gagnon, G. A., Campbell, D. R., & Clark, S. C. (2011). Assessment of hydraulic flocculation processes using cfd. *Journal - American Water Works Association 103*, 66–80. DOCKEY:0074814.

Wilcox, D. (1998). *Turbulence Modeling for CFD*. (2nd ed.). DCW Industries.

World Health Organization (2014). Preventing diarrhoea through better water, sanitation and hygiene.